Uplink Performance Analysis of UAV User Equipments in Dense Cellular Networks

Ziyan Yin*, Jun Li*, Ming Ding†, Feng Shu*, Fei Song*, Yuwen Qian*, and David López-Pérez‡
*The School of Electronic and Optical Engineering,
Nanjing University of Science and Technology, Nanjing 210094
†Data61, CSIRO, Sydney, N.S.W. 2015, Australia
‡Nokia Bell Labs, Dublin 15, Ireland
{ziyan.yin,jun.li,feng.shu,fei.song,admon}@njust.edu.cn, ming.ding@data61.csiro.au, dr.david.lopez@ieee.org

***Abstract*—Unmanned aerial vehicles (UAVs) are envisaged to play a new and important role in future cellular networks. In this paper, we analyze the uplink performance of heterogeneous networks with UAVs in terms of coverage probability and area spectral efficiency (ASE). To be more specific, we first investigate the system performance under a general channel model, with practical considerations such as *(1)* line-of-sight and non-line-of-sight components, *(2)* antenna height difference L between the UAVs and the base stations (BSs), and *(3)* idle mode capabilities (IMCs) at the BSs to mitigate inter-cell interference. Thereafter, we study the system performance under the latest UAV path loss model defined by the 3rd Generation Partnership Project. Under this special case, we provide a more detailed analysis of the coverage probability as well as the ASE, and explore the impacts of difference system parameters on the system performance. Numerical results validate the analytical expressions and show that *(1)* the IMC can improve the coverage probability and the ASE, especially when the network is dense, *(2)* the overall system performance degrades when L increases, and *(3)* the fractional power control factor has a negligible impact on the UAVs performance when L is large enough.**

I. Introduction

Unmanned aerial vehicles (UAVs) have attracted much attention recently, being of use now in many scenarios such as search and rescue, wildlife and nature conservation and inspection [1, 2]. Due to their swift deployment and controllable mobility in three-dimensional (3D) space, UAVs can also be used as an enabling technology in wireless communications.

In recent years, many articles have studied the performance of UAVs from a cellular perspective, most of them considering UAVs as aerial relay base stations (BSs) [1–4]. In these works, the main objective is usually to derive the right number and position of UAV relay BSs to optimise the coverage and/or the capacity of ground user equipment (UE) in different scenarios.

On the other hand, more and more applications can benefit from using UAVs, not as BSs, but as end-users. In this light, a reliable command and control channel for these UAVs is important. To enable a realistic analysis, in [5], the authors discussed the radio propagation characteristics of BS-to-UAV radio channels, while in [6], the authors studied the UAV performance in a multi-UAV scenario. However, these works only considered simplistic single-slope path loss models, ignoring for example the importance of line-of-sight (LoS) and non-line-of-sight (NLoS) components. To be more realistic, and avoid misleading conclusions, we believe that a more practical channel model should be considered.

Another important aspect is that of the UE density. In [7–9]the authors assumed that the density of ground UEs is much larger than the density of BSs to simplify the analysis. However, this assumption does not apply to the UAV reality, especially in the first few years and in dense cellular networks. With this in mind, the work in [10] analyzed the coverage probability with a finite number of UEs, while the authors in [11] studied the network performance with a finite number of UEs as well as a BS idle mode capability (IMC), both assuming a single-tier cellular network. The IMC means that if a BS has no UE communicating with it at a particular moment, the BS can be turned off. Embracing this feature, Chuan *et al.* [12] extended the analysis from single-tier to multi-tier networks, while considering both a finite UE density and the IMC. However, these studies focused on the downlink (DL) performance and they were not targeted to UAVs.

In this paper, we focus on the uplink (UL) performance of homogeneous networks in terms of coverage probability and area spectral efficiency (ASE), with UAV acting as UEs. Moreover, we consider LoS and NLoS transmissions to make the results more practical. Due to the low ratio of the UAV density to the BS density, we also adopt the IMC. The main contributions of this paper are as follows:

- We derive the expressions of the UL coverage probability and the ASE, considering a path loss model that incorporates both the LoS and NLoS transmissions and is dependent of the UAV height.
- We investigate the impact of different parameters on UL network performance, such as the UAV height, the BS density and the UL fractional power control (FPC) factor.
- We also study the UL performance difference between BSs with and without IMC.

II. System Model

We consider an UL cellular network consisting of multiple UAVs and BSs. In the model, the BSs are modelled as a homogeneous Poisson point process (HPPP) Φ_B with density λ BSs/km^2. Similarly, the UAVs are modelled as an HPPP, denoted as Φ_U with intensity ρ UEs/km^2. In previous articles, it was usually assumed that $\rho \gg \lambda$, so that it is safe to consider that each BS has at least one associated UE in its coverage area at any time. However, considering that the application of UAVs as UEs is in its infancy, the UAV density ρ is finite and not sufficiently larger than the BS density λ in our model.

978-1-5386-8088-9/19/$31.00 ©2019 IEEE

Based on this UAV density assumption, a BS with the IMC will enter in idle mode when it has no associated UAV. Thus, the density of active BSs mainly depends on the distribution of UAV and the UAV association strategy (UAS). Considering the existence of LoS and NLoS, we adopt an UAS in which each UAV is connected to the BS with the smallest path loss, and an UAV will only be associated with a BS at the same time. Thus, the density of active BSs is at most equal to the density of active UAVs. As the UAVs and the BSs are randomly and uniformly distributed, it is safe to assume that the distributions of the active UAVs and BSs are also HPPPs. The density of active BSs $\widetilde{\lambda}$ can be derived as

$$\widetilde{\lambda} = \lambda \left[1 - \frac{1}{\left(1 + \frac{\rho}{q\lambda}\right)^{q}} \right], \tag{1}$$

where the value of q depends on the path loss model, and $q = 3.5$, as recommended in [13, 14].

Without loss of generality, we randomly choose an active BS to be the typical BS, and assume it is at the origin. The UAV communicating with the typical BS is referred to as the typical UAV. Simultaneously, other UAVs communicating with other BSs are the interferers as shown in Fig. 1.

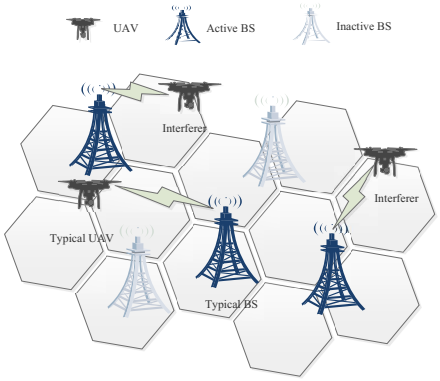

Fig. 1. An UL cellular network consisting of multiple UAVs and BSs.

Also note that the UAV and BS heights are denoted by h_{UT} and h_{BS}, respectively, while the two-dimensional (2D) distance between an UAV and a BS is denoted by r. Thus, the absolute height difference can be calculated by $L = h_{\mathrm{UT}} - h_{\mathrm{BS}}$, while their 3D distance can be computed as $\omega = \sqrt{r^2 + L^2}$.

A general path loss model $\zeta(\omega)$ is adopted,

$$\zeta(\omega) = \begin{cases} \zeta_1(\omega), & 0 < \omega \le d_1 \\ \zeta_2(\omega), & d_1 < \omega \le d_2 \\ \vdots & \vdots \\ \zeta_N(\omega), & \omega > d_{N-1} \end{cases}, \tag{2}$$

where $\zeta_n(\omega)$, $n \in \{1, 2, \ldots, N\}$ can be written as

$$\zeta_n(\omega) = A_n^{\mathrm{Path}} \omega^{\alpha_n^{\mathrm{Path}}}, \tag{3}$$

where $\mathrm{Path} \in \{\mathrm{L}, \mathrm{NL}\}$ represents the LoS and the NLoS cases, respectively, A_n^{Path} is the path loss at the distance of 1 meter, and α_n^{Path} is the path loss exponent. $\Pr^{\mathrm{Path}}(\omega)$ is the probability of having a LoS or NLoS case, where

$$\Pr^{\mathrm{Path}}(\omega) = \begin{cases} \Pr_1^{\mathrm{Path}}(\omega), & 0 < \omega \le d_1 \\ \Pr_2^{\mathrm{Path}}(\omega), & d_1 < \omega \le d_2 \\ \vdots & \vdots \\ \Pr_N^{\mathrm{Path}}(\omega), & \omega > d_{N-1} \end{cases}. \tag{4}$$

Moreover, we consider the following assumptions. First, each BS and each UAV in the network are equipped with an isotropic antenna. Second, the multi-path fading is modelled as independently identical distributed Rayleigh fading.

In addition, the transmission power of an UAV k is denoted as

$$P_k = B\zeta(\omega)^{\epsilon}, \tag{5}$$

where B is the baseline power, and $\epsilon \in (0, 1]$ represents the FPC factor. In contrast, the received power at the typical BS is denoted as

$$P^{\mathrm{rx}} = B\zeta(\omega)^{(\epsilon-1)} g_0, \tag{6}$$

where g_0 is the channel gain, and $g_0 \sim \exp(1)$.

III. Main Results

In this section, we use a 3D stochastic geometry analysis to study the performance of the presented network in terms of the coverage probability and the ASE.

A. The Coverage Probability

The coverage probability is defined as the probability that the UAV signal to interference plus noise ration (SINR) at the typical BS is larger than a pre-designated threshold.

$$P^{\mathrm{cov}}(\lambda, \tau) = \Pr[\mathrm{SINR} > \tau], \tag{7}$$

where τ is the pre-designated SINR threshold, and the UAV SINR can be written as

$$\mathrm{SINR} = \frac{P^{\mathrm{rx}}}{I_Z + \sigma^2}, \tag{8}$$

where σ^2 is the noise power, Z is the set of interferers, and I_Z is the interference, which is given by

$$I_Z = \sum_{z \in Z} B\zeta\left(\omega_z^{\mathrm{S}}\right)^{\epsilon} \zeta\left(\omega_z^{\mathrm{T}}\right)^{-1} g_z. \tag{9}$$

where ω_z^{S} and ω_z^{T} are the distances from the UAV z to its serving BS and the typical BS, respectively, and g_z is the channel gain between the UAV z and the typical BS.

According to our segmented path loss model and UAS, which considers LoS and NLoS, the main results of coverage probability $P^{\mathrm{cov}}(\lambda, \tau)$ are shown in Theorem 1.

Theorem 1: The coverage probability $P^{\mathrm{cov}}(\lambda, \tau)$ can be derived as

$$P^{\mathrm{cov}}(\lambda, \tau) = \sum_{n=1}^{N} \left(T_n^{\mathrm{L}} + T_n^{\mathrm{NL}}\right). \tag{10}$$

In (10), we have

$$T_n^{\mathrm{Path}} = \int_{\sqrt{d_{n-1}^2 - L^2}}^{\sqrt{d_n^2 - L^2}} \Pr\left[\frac{B\zeta(\omega)^{(\epsilon-1)} g}{I_Z + \sigma^2} > \tau \middle| \mathrm{Path} \right] \times f_{\omega,n}^{\mathrm{Path}}(r)\, \mathrm{d}r, \tag{11}$$

where d_0 and d_N are L and $+\infty$, respectively.

Note that $f_{\omega,n}^{\mathrm{L}}(r)$ and $f_{\omega,n}^{\mathrm{NL}}(r)$ are given by the following equations as

$$\begin{aligned} f_{\omega,n}^{\mathrm{L}}(r) &= \exp\left(-\int_0^r \Pr^{\mathrm{L}}\left(\sqrt{u^2+L^2}\right)2\pi u\lambda \mathrm{d}u\right) \\ &\times \exp\left(-\int_0^{r_1}\left(1-\Pr^{\mathrm{L}}\left(\sqrt{u^2+L^2}\right)\right)2\pi u\lambda \mathrm{d}u\right) \\ &\times \Pr^{\mathrm{L}}\left(\sqrt{r^2+L^2}\right)2\pi r\lambda, \end{aligned} \tag{12}$$

and

$$\begin{aligned} f_{\omega,n}^{\mathrm{NL}}(r) &= \exp\left(-\int_0^{r_2} \Pr^{\mathrm{L}}\left(\sqrt{u^2+L^2}\right)2\pi u\lambda \mathrm{d}u\right) \\ &\times \exp\left(-\int_0^{r}\left(1-\Pr^{\mathrm{L}}\left(\sqrt{u^2+L^2}\right)\right)2\pi u\lambda \mathrm{d}u\right) \\ &\times \left(1-\Pr^{\mathrm{L}}\left(\sqrt{r^2+L^2}\right)\right)2\pi r\lambda, \end{aligned} \tag{13}$$

where

$$r_1 = \sqrt{\left(\frac{A^{\mathrm{L}}(r^2+L^2)^{\frac{\alpha^{\mathrm{L}}}{2}}}{A^{\mathrm{NL}}}\right)^{\frac{2}{\alpha^{\mathrm{NL}}}} - L^2}, \tag{14}$$

and

$$r_2 = \sqrt{\left(\frac{A^{\mathrm{NL}}(r^2+L^2)^{\frac{\alpha^{\mathrm{NL}}}{2}}}{A^{\mathrm{L}}}\right)^{\frac{2}{\alpha^{\mathrm{L}}}} - L^2}. \tag{15}$$

In addition, $\Pr\left[\frac{B\zeta(\omega)^{(\epsilon-1)}g}{I_Z+\sigma^2} > \tau \middle| \mathrm{Path}\right]$ *can be derived as*

$$\begin{aligned} &\Pr\left[\frac{B\zeta(\omega)^{(\epsilon-1)}g}{I_Z+\sigma^2} > \tau \middle| \mathrm{Path}\right] = \\ &\exp\left(-\frac{\tau\sigma^2}{B\left(A^{\mathrm{Path}}\omega^{\alpha^{\mathrm{Path}}}\right)^{(\epsilon-1)}}\right)\mathcal{L}_{I_Z}\left(\frac{\tau}{B\left(A^{\mathrm{Path}}\omega^{\alpha^{\mathrm{Path}}}\right)^{(\epsilon-1)}}\right), \end{aligned} \tag{16}$$

where when the path link is LoS, $\mathcal{L}_{I_Z}^{\mathrm{L}}(s)$ can be derived as

$$\begin{aligned} \mathcal{L}_{I_Z}^{\mathrm{L}}(s) &= \exp\left\{-2\pi\widetilde{\lambda}\int_r^\infty \Pr^{\mathrm{L}}\left(\sqrt{x^2+L^2}\right)\right. \\ &\left.\times\left(\int_0^\infty f(u,x)\, f_\omega^{\mathrm{L}}(u)\,\mathrm{d}u \middle| \mathrm{LoS}\right)\mathrm{d}x\right\} \\ &\times \exp\left\{-2\pi\widetilde{\lambda}\int_{r_1}^\infty \Pr^{\mathrm{NL}}\left(\sqrt{x^2+L^2}\right)\right. \\ &\left.\times\left(\int_0^\infty f(u,x)\, f_\omega^{\mathrm{NL}}(u)\,\mathrm{d}u \middle| \mathrm{NLoS}\right)\mathrm{d}x\right\}, \end{aligned} \tag{17}$$

and when the path link is NLoS, $\mathcal{L}_{I_Z}^{\mathrm{NL}}(s)$ can be derived as

$$\begin{aligned} \mathcal{L}_{I_Z}^{\mathrm{NL}}(s) &= \exp\left\{-2\pi\widetilde{\lambda}\int_{r_2}^\infty \Pr^{\mathrm{L}}\left(\sqrt{x^2+L^2}\right)\right. \\ &\left.\times\left(\int_0^\infty f(u,x)\, f_\omega^{\mathrm{L}}(u)\,\mathrm{d}u \middle| \mathrm{LoS}\right)\mathrm{d}x\right\} \\ &\times \exp\left\{-2\pi\widetilde{\lambda}\int_{r}^\infty \Pr^{\mathrm{NL}}\left(\sqrt{x^2+L^2}\right)\right. \\ &\left.\times\left(\int_0^\infty f(u,x)\, f_\omega^{\mathrm{NL}}(u)\,\mathrm{d}u \middle| \mathrm{NLoS}\right)\mathrm{d}x\right\}, \end{aligned} \tag{18}$$

where

$$f(u,x) = \frac{1}{1+s^{-1}B^{-1}\zeta\left(\sqrt{u^2+L^2}\right)^{-\epsilon}\zeta\left(\sqrt{x^2+L^2}\right)}. \tag{19}$$

Proof: Due to the page limit, we omit the proof and will provide it in the journal version of this work. ■

Note that the difference between the DL and UL analysis in Theorem 1 is mainly in the Laplace transform of I_Z shown in (17) and (18), where an additional integral with respect to the distance ω_z^{S} is required in the UL case.

B. The Area Spectral Efficiency

The ASE in bps/Hz/km^2 can be mathematically defined as

$$A^{\mathrm{ASE}}(\lambda,\tau_0) = \widetilde{\lambda}\int_{\tau_0}^\infty \log_2(1+\gamma) f_\Gamma(\lambda,\gamma)\,\mathrm{d}\gamma, \tag{20}$$

where τ_0 is the pre-defined minimum working SINR, and $f_\Gamma(\lambda,\gamma)$ is the probability density function (PDF) of the SINR observed at the typical BS, which can be written as

$$f_\Gamma(\lambda,\gamma) = \frac{\partial\left(1-P^{\mathrm{cov}}(\lambda,\gamma)\right)}{\partial\gamma}. \tag{21}$$

From Theorem 1, we can see that some equations are function of the BS density λ, e.g. the expressions of (12) and (13), while some others are function of the active BS density $\widetilde{\lambda}$, e.g. the expressions of (17) and (18). The reasons for being function of different BS densities are as follows:

1) According to the UAS, each UAV should associate with the BS which can offer the smallest path loss. Thus, each UAV compares all the BSs, and chooses its serving BS. (12) and (13) show the impact of the serving BS selection. Obviously, we should use λ instead of $\widetilde{\lambda}$.
2) The impact of the aggregate interference power is measured in (17) and (18). Based on the definition of interferer, we know that only UAVs transmitting can cause interference, and that the amount of simultaneous UAVs transmitting defines the amount of active BSs, which equals to $\widetilde{\lambda}$.

Based on the above discussion, we have the following two remarks.

Remark 1: For the coverage probability and the ASE without IMC, we can simply replace $\widetilde{\lambda}$ with λ in eqs. (10) and (20).

Remark 2: The coverage probability is always larger when considering the IMC. This is because a) $\widetilde{\lambda} < \lambda$ *and* $\widetilde{\lambda} < \rho$*;* b) $\exp(-x)$ *is a decreasing function in eqs. (17) and (18); and* c) $\mathcal{L}_{I_Z}(s)$ *decreases as the active BS density increases.*

IV. Analysis Based on the 3GPP Spacial Case

Based on the 3GPP recommendations [15], we adopt the following case to show our analytical results, where the path loss model is a two-piece function, and can be expressed as

$$\zeta(\omega) = \begin{cases} A^{\mathrm{L}}\omega^{\alpha^{\mathrm{L}}}, & \mathrm{LoS}:\Pr^{\mathrm{L}}(r) \\ A^{\mathrm{NL}}\omega^{\alpha^{\mathrm{NL}}}, & \mathrm{NLoS}:\left(1-\Pr^{\mathrm{L}}(r)\right) \end{cases}. \tag{22}$$

Note that the probability function in (22) depends on 2D distances instead of 3D ones, and can be defined as [15]

$$\Pr^{\mathrm{L}}(r) = \begin{cases} 1, & r \le d \\ \frac{d}{r} + \exp\left(-\frac{r}{p}\right)\left(1-\frac{d}{r}\right), & r > d \end{cases}, \tag{23}$$

where $d = \max\left(294.05\log_{10}(L) - 432.94, 18\right)$ is the smallest NLoS link distance, and $p = 233.98\log_{10}(L) - 0.95$.

Combining Theorem 1 with this special case, we can get that

$$P^{\mathrm{cov}}(\lambda,\tau) = \sum_{n=1}^{2}\left(T_n^{\mathrm{L}} + T_n^{\mathrm{NL}}\right). \tag{24}$$

As mentioned before, the coverage probability $P^{\mathrm{cov}}(\lambda,\tau)$ is a function of the PDF of UAV to BS distance, and according to this path loss model, the PDF of the distance from the interferer UAV to its serving BS u can divide into 3 cases.

Case 1: When the path between the interferer UAV and the typical BS is LoS, and the distance $x \le d$, $f^{\mathrm{L}}_{\omega,1}(u)$ can be derived as

$$f^{\mathrm{L}}_{\omega,1}(u) = 2\pi u\lambda \exp\left(-\pi\lambda u^2\right). \tag{25}$$

Case 2: When the path between the interferer UAV and the typical BS is LoS, and the distance $x > d$, $f^{2\mathrm{L}}_{\omega}(u)$ can be derived as

$$f^{2\mathrm{L}}_{\omega}(u) = \begin{cases} \begin{cases} f^{\mathrm{L}}_{\omega,1}(u), & \mathrm{LoS}, \quad 0 < u \le d, \\ f^{2\mathrm{L}}_{\omega,1}(u), & \mathrm{LoS}, \quad d < u \le x, \end{cases} & d < x \le y_2 \\ \begin{cases} f^{\mathrm{L}}_{\omega,1}(u), & \mathrm{LoS}, \quad 0 < u \le d, \\ f^{2\mathrm{L}}_{\omega,1}(u), & \mathrm{LoS}, \quad d < u \le y_2, \\ f^{2\mathrm{L}}_{\omega,2}(u), & \mathrm{LoS}, \quad y_2 < u \le x, \\ f^{\mathrm{NL}}_{\omega,2}(u), & \mathrm{NLoS}, \quad d < u \le x_1, \end{cases} & x > y_2 \end{cases}, \tag{26}$$

where $y_2 = \sqrt{\left(\frac{A^{\mathrm{NL}}(d^2+L^2)^{\frac{\alpha^{\mathrm{NL}}}{2}}}{A^{\mathrm{L}}}\right)^{\frac{2}{\alpha^{\mathrm{L}}}} - L^2}$, and $x_1 = \sqrt{\left(\frac{A^{\mathrm{L}}(x^2+L^2)^{\frac{\alpha^{\mathrm{L}}}{2}}}{A^{\mathrm{NL}}}\right)^{\frac{2}{\alpha^{\mathrm{NL}}}} - L^2}$.

In (26), we have

$$\begin{aligned} f^{2\mathrm{L}}_{\omega,1}(u) = \exp\Bigg(-2\pi\lambda\Bigg(&p(d-p-u)\exp\left(-\frac{u}{p}\right) \\ &+ ud - \frac{1}{2}d^2 + p^2\exp\left(-\frac{d}{p}\right)\Bigg)\Bigg) \\ &\times\left(d+\exp\left(-\frac{u}{p}\right)(u-d)\right)2\pi\lambda, \end{aligned} \tag{27}$$

$$\begin{aligned} f^{2\mathrm{L}}_{\omega,2}(u) = \exp\Bigg(-2\pi\lambda\Bigg(&\frac{1}{2}u_1^2 + d(u-u_1) \\ &+ p(d-p-u)\exp\left(-\frac{u}{p}\right) \\ &- p(d-p-u_1)\exp\left(-\frac{u_1}{p}\right)\Bigg)\Bigg) \\ &\times\left(d+\exp\left(-\frac{u}{p}\right)(u-d)\right)2\pi\lambda, \end{aligned} \tag{28}$$

$$\begin{aligned} f^{\mathrm{NL}}_{\omega,2}(u) = \exp\Bigg(-2\pi\lambda\Bigg(&\frac{1}{2}u^2 + d(u_2-u) \\ &+ p(d-p-u_2)\exp\left(-\frac{u_2}{p}\right) \\ &- p(d-p-u)\exp\left(-\frac{u}{p}\right)\Bigg)\Bigg) \\ &\times\left(u-d-\exp\left(-\frac{u}{p}\right)(u-d)\right)2\pi\lambda, \end{aligned} \tag{29}$$

where $u_1 = \sqrt{\left(\frac{A^{\mathrm{L}}(u^2+L^2)^{\frac{\alpha^{\mathrm{L}}}{2}}}{A^{\mathrm{NL}}}\right)^{\frac{2}{\alpha^{\mathrm{NL}}}} - L^2}$, and $u_2 = \sqrt{\left(\frac{A^{\mathrm{NL}}(u^2+L^2)^{\frac{\alpha^{\mathrm{NL}}}{2}}}{A^{\mathrm{L}}}\right)^{\frac{2}{\alpha^{\mathrm{L}}}} - L^2}$.

Case 3: When the path between the interferer UAV and the typical BS is NLoS, and the distance $x > d$, $f^{2\mathrm{NL}}_{\omega}(u)$ can be derived as

$$f^{2\mathrm{NL}}_{\omega}(u) = \begin{cases} f^{\mathrm{L}}_{\omega,1}(u), & \mathrm{LoS}, & 0 < u \le d \\ f^{2\mathrm{L}}_{\omega,1}(u), & \mathrm{LoS}, & d < u \le y_2 \\ f^{2\mathrm{L}}_{\omega,2}(u), & \mathrm{LoS}, & y_2 < u \le x_2 \\ f^{\mathrm{NL}}_{\omega,2}(u), & \mathrm{NLoS}, & d < u \le x \end{cases}, \tag{30}$$

where $x_2 = \sqrt{\left(\frac{A^{\mathrm{NL}}(x^2+L^2)^{\frac{\alpha^{\mathrm{NL}}}{2}}}{A^{\mathrm{L}}}\right)^{\frac{2}{\alpha^{\mathrm{L}}}} - L^2}$.

T^{L}_1, T^{NL}_1, T^{L}_2 and T^{NL}_2 respectively relate to the coverage probability when the typical UAV is communicating with the typical BS with a LoS or a NLoS link of different distance, and we investigate these in the following subsections.

A. The Result of T^{L}_1

Lemma 1: The coverage probability T^{L}_1 can be written as

$$\begin{aligned} T^{\mathrm{L}}_1 = &\int_0^d e^{-\frac{\tau\sigma^2}{B\left(A^{\mathrm{L}}\omega^{\alpha^{\mathrm{L}}}\right)^{(\epsilon-1)}}}\mathcal{L}_{I_Z}\left(\frac{\tau}{B\left(A^{\mathrm{L}}\omega^{\alpha^{\mathrm{L}}}\right)^{(\epsilon-1)}}\right) \\ &\times f^{\mathrm{L}}_{\omega,1}(r)\,\mathrm{d}r, \end{aligned} \tag{31}$$

and $\mathcal{L}_{I_Z}(s)$ can be written as

$$\begin{aligned} &\mathcal{L}_{I_Z}(s) \\ &= \exp\left\{-2\pi\widetilde{\lambda}\int_r^d\left(\int_0^\infty f(u,x)\,f^{1\mathrm{L}}_{\omega}(u)\,\mathrm{d}u\middle|\,\mathrm{LoS}\right)x\mathrm{d}x\right\} \\ &\times\exp\left\{-2\pi\widetilde{\lambda}\int_d^\infty\left(d+\exp\left(-\frac{x}{p}\right)(x-d)\right)\right. \\ &\left.\times\left(\int_0^\infty f(u,x)\,f^{2\mathrm{L}}_{\omega}(u)\,\mathrm{d}u\middle|\,\mathrm{LoS}\right)\mathrm{d}x\right\} \\ &\times\exp\left\{-2\pi\widetilde{\lambda}\int_d^\infty\left(x-d-\exp\left(-\frac{x}{p}\right)(x-d)\right)\right. \\ &\left.\times\left(\int_0^\infty f(u,x)\,f^{2\mathrm{NL}}_{\omega}(u)\,\mathrm{d}u\middle|\,\mathrm{NLoS}\right)\mathrm{d}x\right\}. \end{aligned} \tag{32}$$

B. The Result of T^{NL}_1

Since

$$\begin{aligned} f^{\mathrm{NL}}_{\omega,1}(r) &= \exp\left(-\int_0^{r_2}2\pi u\lambda\mathrm{d}u\right) \\ &\times\exp\left(-\int_0^r 0\times 2\pi u\lambda\mathrm{d}u\right)\times 0\times 2\pi r\lambda \\ &= 0, \end{aligned} \tag{33}$$

we have

$$\begin{aligned} T^{\mathrm{NL}}_1 = &\int_0^d e^{-\frac{\tau\sigma^2}{B\left(A^{\mathrm{NL}}\omega^{\alpha^{\mathrm{NL}}}\right)^{(\epsilon-1)}}} \\ &\times\mathcal{L}_{I_Z}\left(\frac{\tau}{B\left(A^{\mathrm{NL}}\omega^{\alpha^{\mathrm{NL}}}\right)^{(\epsilon-1)}}\right)f^{\mathrm{NL}}_{\omega,1}(r)\,\mathrm{d}r = 0. \end{aligned} \tag{34}$$

C. The Result of T_2^{L}

Lemma 2: The coverage probability T_2^{L} can be written as

$$T_2^{\mathrm{L}} = \int_d^{\infty} e^{-\frac{\tau\sigma^2}{B\left(A^{\mathrm{L}}\omega^{\alpha^{\mathrm{L}}}\right)^{(\epsilon-1)}}} \mathcal{L}_{I_Z}\left(\frac{\tau}{B\left(A^{\mathrm{L}}\omega^{\alpha^{\mathrm{L}}}\right)^{(\epsilon-1)}}\right) \times f_{\omega}^{2\mathrm{L}}(r)\,\mathrm{d}r, \tag{35}$$

where

$$f_{\omega}^{2\mathrm{L}}(r) = \begin{cases} f_{\omega,1}^{2\mathrm{L}}(r), & d < r \le y_2 \\ f_{\omega,2}^{2\mathrm{L}}(r), & r > y_2 \end{cases}, \tag{36}$$

and $\mathcal{L}_{I_Z}(s)$ for $d < r \le y_2$ and $r > y_2$ are respectively denoted as

$$\begin{aligned}\mathcal{L}_{I_Z}(s) = &\exp\left\{-2\pi\widetilde{\lambda}\int_r^{\infty}\left(d+\exp\left(-\frac{x}{p}\right)(x-d)\right)\right.\\ &\left.\times\left(\int_0^{\infty} f(u,x)\, f_{\omega}^{2\mathrm{L}}(u)\,\mathrm{d}u\middle|\,\mathrm{LoS}\right)\mathrm{d}x\right\}\\ &\times\exp\left\{-2\pi\widetilde{\lambda}\int_d^{\infty}\left(x-d-\exp\left(-\frac{x}{p}\right)(x-d)\right)\right.\\ &\left.\times\left(\int_0^{\infty} f(u,x)\, f_{\omega}^{2\mathrm{NL}}(u)\,\mathrm{d}u\middle|\,\mathrm{NLoS}\right)\mathrm{d}x\right\},\end{aligned} \tag{37}$$

and

$$\begin{aligned}\mathcal{L}_{I_Z}(s) = &\exp\left\{-2\pi\widetilde{\lambda}\int_r^{\infty}\left(d+\exp\left(-\frac{x}{p}\right)(x-d)\right)\right.\\ &\left.\times\left(\int_0^{\infty} f(u,x)\, f_{\omega}^{2\mathrm{L}}(u)\,\mathrm{d}u\middle|\,\mathrm{LoS}\right)\mathrm{d}x\right\}\\ &\times\exp\left\{-2\pi\widetilde{\lambda}\int_{r_1}^{\infty}\left(x-d-\exp\left(-\frac{x}{p}\right)(x-d)\right)\right.\\ &\left.\times\left(\int_0^{\infty} f(u,x)\, f_{\omega}^{2\mathrm{NL}}(u)\,\mathrm{d}u\middle|\,\mathrm{NLoS}\right)\mathrm{d}x\right\}.\end{aligned} \tag{38}$$

D. The Result of T_2^{NL}

Lemma 3: The coverage probability T_2^{NL} can be written as

$$T_2^{\mathrm{NL}} = \int_d^{\infty} e^{-\frac{\tau\sigma^2}{B\left(A^{\mathrm{NL}}(\omega)^{\alpha^{\mathrm{NL}}}\right)^{(\epsilon-1)}}} \times \mathcal{L}_{I_Z}\left(\frac{\tau}{B\left(A^{\mathrm{NL}}(\omega)^{\alpha^{\mathrm{NL}}}\right)^{(\epsilon-1)}}\right) f_{\omega,2}^{\mathrm{NL}}(r)\,\mathrm{d}r, \tag{39}$$

and $\mathcal{L}_{I_Z}(s)$ can be written as

$$\begin{aligned}\mathcal{L}_{I_Z}(s) = &\exp\left\{-2\pi\widetilde{\lambda}\int_{r_2}^{\infty}\left(d+\exp\left(-\frac{x}{p}\right)(x-d)\right)\right.\\ &\left.\times\left(\int_0^{\infty} f(u,x)\, f_{\omega}^{2\mathrm{L}}(u)\,\mathrm{d}u\middle|\,\mathrm{LoS}\right)\mathrm{d}x\right\}\\ &\times\exp\left\{-2\pi\widetilde{\lambda}\int_r^{\infty}\left(x-d-\exp\left(-\frac{x}{p}\right)(x-d)\right)\right.\\ &\left.\times\left(\int_0^{\infty} f(u,x)\, f_{\omega}^{2\mathrm{NL}}(u)\,\mathrm{d}u\middle|\,\mathrm{NLoS}\right)\mathrm{d}x\right\}.\end{aligned} \tag{40}$$

V. Simulations and Discussions

In this section, we investigate the UL network performance in terms of coverage probability and ASE, and use both numerical and simulation results to establish the accuracy of our analysis. The parameters in our paper come from [15], and are as follows: $\alpha^{\mathrm{L}} = 2.225 - 0.05\log_{10}(h_{\mathrm{UT}})$, $\alpha^{\mathrm{NL}} = 4.32 - 0.76\log_{10}(h_{\mathrm{UT}})$, $A^{\mathrm{L}} = 10^{10.3692}$, $A^{\mathrm{NL}} = 10^{3.842}$, $P_0 = -76$ dBm, $\sigma^2 = -99$ dBm, and $h_{\mathrm{BS}} = 10$ m.

A. Validation of the Analytical Results of $P^{\mathrm{cov}}(\lambda,\tau)$

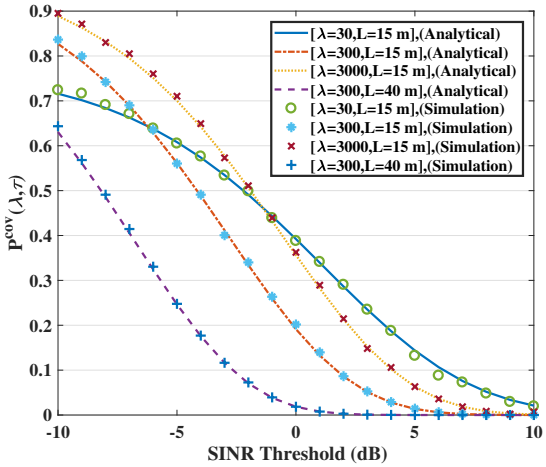

Fig. 2. $P^{\mathrm{cov}}(\lambda,\tau)$ vs. τ with $\epsilon = 0.9$ and $\rho = 300$ UEs/km^2.

In Fig. 2, we plot the coverage probability $P^{\mathrm{cov}}(\lambda,\tau)$ versus the SINR threshold τ, with $\epsilon = 0.9$ and $\rho = 300$ UEs/km^2. The analytical results are based on the analysis in Section IV, while the simulation results are collected from Monte Carlo simulations. To validate the correctness of our analysis, we consider various scenarios, such as different UAV-to-BS antenna height differences and different BS densities.

From Fig. 2, we can see that our analytical results match the simulation results well, thus indicating the accuracy of our analysis. As a result, we only use analytical results of the coverage probability $P^{\mathrm{cov}}(\lambda,\tau)$ in our discussion hereafter.

The observations based on Fig. 2 are as follows:

- The coverage probability $P^{\mathrm{cov}}(\lambda,\tau)$ decreases with an increasing τ, and approaches zero faster as τ grows.
- For $L = 15$ m, when τ is small, e.g., $\tau < -5$ dB, the coverage probability of a dense network (with a larger λ) is better than that of a sparse network. This is because the signal power plays a major role, as a large amount of interference can be tolerated. However, when $\tau > 0$ dB, the coverage probability with $\lambda = 30$ BSs/km^2 is better than that with $\lambda = 300$ or 3000 BSs/km^2. This is because the interference power plays a major role, and there are more interferers with the more aggressive spatial reuse.
- When the BS density $\lambda = 300$ BSs/km^2, the coverage probability $P^{\mathrm{cov}}(\lambda,\tau)$ with $L = 40$ m is smaller than that with $L = 15$ m, and the former reduces to zero faster. This is because many interferers turn from NLoS to LoS, due to the higher height of the interferers overlooking larger areas.

B. The Results of $P^{\text{cov}}(\lambda, \tau)$ vs. L

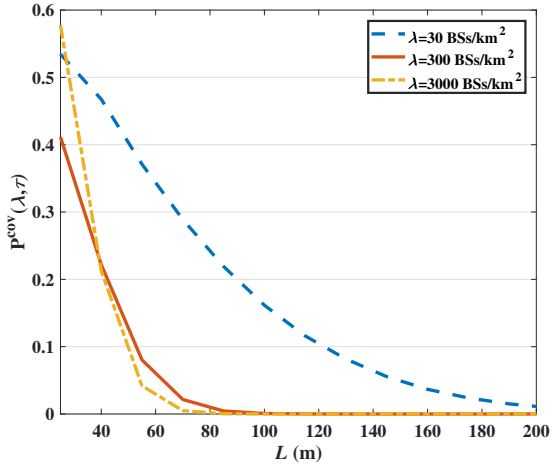

Fig. 3. $P^{\text{cov}}(\lambda, \tau)$ vs. L with $\tau = -3$ dB, $\epsilon = 0.9$ and $\rho = 300$ UEs/km^2.

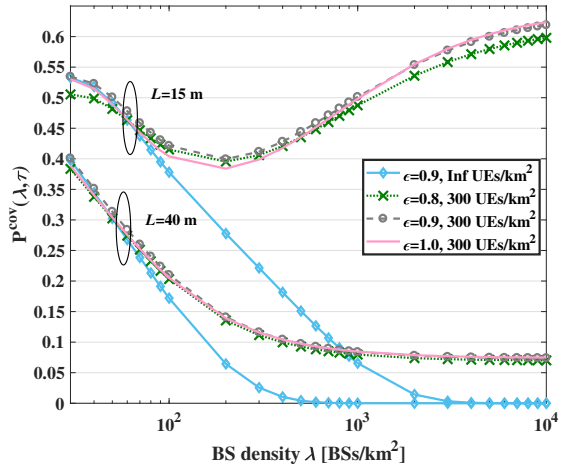

Fig. 4. $P^{\text{cov}}(\lambda, \tau)$ vs. λ with $\tau = -3$ dB.

In Fig. 3, we show the results of coverage probability with $\tau = -3$ dB, $\epsilon = 0.9$ and $\rho = 300$ UEs/km^2 versus various UAV-to-BS antenna height differences L. Some interesting observations are as follows:

- The coverage probability $P^{\text{cov}}(\lambda, \tau)$ decreases as UAVs fly higher, especially in dense networks (large λ), where $P^{\text{cov}}(\lambda, \tau)$ almost crashes to zero when $L > 90$ m, implying a total network outage.
- The denser the network, the faster the coverage probability decreases as L increases. This is again due to the more interferers and the larger LoS probability with the BS density and the UAV height, respectively. This is in line with the results of Fig. 2.

As can be observed in Fig. 3, when $L > 50$ m, the coverage probability is smaller than 0.2, which is rather poor. To ensure good network performance, we only consider $L < 50$ m hereafter.

C. The Results of $P^{\text{cov}}(\lambda, \tau)$ vs. λ

In Fig. 4, we show the results of coverage probability with $\tau = -3$ dB and for various BS densities. We focus on three comparisons:

1) For a certain L, e.g., 15 m or 40 m, the coverage probability of an infinite UAVs density approaches zero when the network is ultra dense, which is referred to as *the ASE Crash* in [7, 16]. In contrast, when the UAV density is finite, the number of interferers is also finite, and thus the coverage probability becomes better.
2) For $L = 15$ m and $\rho = 300$ UEs/km^2, we can see that:
   - When the network is relatively sparse, e.g. $\lambda < \rho$, the coverage probability decreases as the BS density increases. This is because when the BS density increases, the scenario is light up with coverage and the number of active UAVs increases, which means the interference received at the typical BS increases too.
   - When the network is dense enough, e.g. $\lambda > \rho$, the coverage probability increases as the BS density increases. Compared with the sparse networks, the number of interferers exhibits a slow pace in the growth rate in dense networks, and their transmit power decreases as they are closer to their servers.
   - No matter whether the network is sparse or dense, the case of $\epsilon = 0.9$ exhibits the best performance among the investigated ceases.
3) For $L = 40$ m and $\rho = 300$ UEs/km^2, the coverage probability monotonically decreases with the increasing BS density, even when the BS density is large enough. This is because the interfering UAVs are now at a much higher height, and thus are always in LoS with the typical BS and they approach it relatively faster with the BS density (the vertical and not the horizontal distance dominates and drives the LoS).

From Fig. 4, we can see that the coverage probability with various UAV heights presents different trends. To further discuss the influence of L, we plot Fig. 5, where $\tau = -3$ dB, $\epsilon = 0.9$, $\rho = 300$ UEs/km^2 and L adopts different values. The observations are as follows:

- When $L \in [15, 35]$ m, the coverage probability increases as the BS density increases in dense network, i.e., $\lambda > 7000$ BSs/km^2, and the growing trend of the coverage probability with a smaller height is more obvious than that with a larger height. This is because the number of interferers exhibits a slow pace in the growth rate in dense networks, and their transmit power decreases as they are closer to their servers.
- When $L > 35$ m, the coverage probability decreases as the BS density increases when $\lambda \in [30, 1000]$ BSs/km^2. The height dominates and drives more and more UAVs as LoS interferers.

D. The Results of $A^{ASE}(\lambda, T_0)$ vs. λ

In Fig. 6, we show the results of ASE with $\tau_0 = 0$ dB and $\epsilon = 0.9$ based on the analytical results of $P^{\text{cov}}(\lambda, \tau)$.

The observations are as follows:

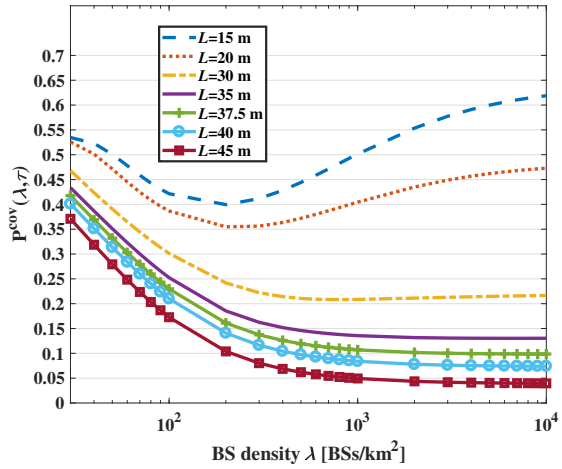

Fig. 5. $P^{\text{cov}}(\lambda, \tau)$ vs. λ with $\tau = -3$ dB.

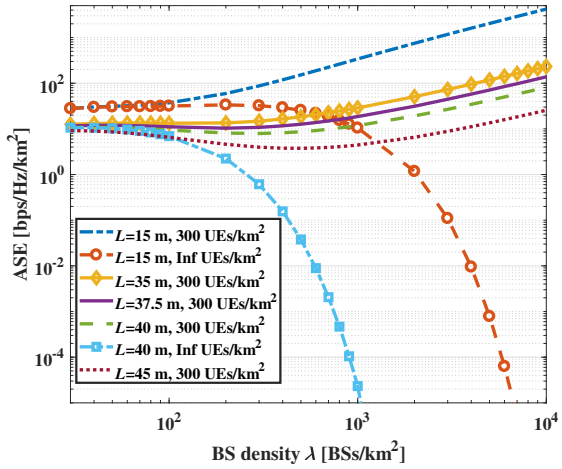

Fig. 6. $A^{\text{ASE}}(\lambda, \tau_0)$ vs. λ with $\tau_0 = 0$ dB, $\epsilon = 0.9$.

- When the UAV density is Inf UEs/km^2, the ASE decreases when the BS density increases, and approaches zero when the BS density is large enough, which is referred to as *the ASE Crash* in [7, 16].
- When the UAV density is 300 UEs/km^2 and the network is sparse, i.e., $\lambda \in [30, 60]$ BSs/km^2, the ASE increases when the BS density increases. This is because the network is generally noise-limited, and the smaller distance from the typical UAV to the typical BS can improve performance. Then, the ASE decreases as the BS density increases when $L \geq 35$ m, while it increases when $L = 15$ m. When the BS density is dense enough, i.e., $\lambda > 1000$ BSs/km^2, the ASE increases as the BS density increases.
- For $L \in [15, 45]$ m, when ρ is the same, the ASE with a larger L is always better than that with a smaller L .

VI. Conclusion

In this paper, we have provided an analytical framework to compute the coverage probability and the ASE in the UL when the UAVs act as UEs and BSs have an IMC. Moreover, we have studied the performance impact of the absolute height difference between the UAV and the UE, considering probabilistic LoS and NLoS transmissions. Such impact is not only quantitative but also qualitative. The coverage probability and the ASE decrease as the UAV-to-BS antenna height difference L increases, which indicates the operators should not place the UAVs at too high altitudes. Thanks to the BS IMC, the coverage probability and the ASE with finite UAVs is much better than that with infinite UAVs. Moreover, we find that the influence of FPC factor is small, and even makes no difference when $L = 40$ m. In our future work, we will consider both aerial UEs and ground UEs, and discuss the influence brought by the aerial UEs to the ground UEs.

References

[1] A. Fotouhi, M. Ding, and M. Hassan, "Flying drone base stations for macro hotspots," *IEEE Access*, vol. 6, pp. 19 530–19 539, 2018.

[2] A. Fotouhi, H. Qiang, M. Ding, M. Hassan, L. G. Giordano, A. Garcia-Rodriguez, and J. Yuan, "Survey on UAV cellular communications: Practical aspects, standardization advancements, regulation, and security challenges," *IEEE Communications Surveys and Tutorials*, [Online]:arXiv:1809.01752 [cs.NI], Sep. 2018.

[3] M. Mozaffari, W. Saad, M. Bennis, and M. Debbah, "Unmanned aerial vehicle with underlaid device-to-device communications: Performance and tradeoffs," *IEEE Transactions on Wireless Communications*, vol. 15, no. 6, pp. 3949–3963, Jun. 2016.

[4] C. Zhang and W. Zhang, "Spectrum sharing for drone networks," *IEEE Journal on Selected Areas in Communications*, vol. 35, no. 1, pp. 136–144, Jan. 2017.

[5] A. Al-Hourani and K. Gomez, "Modeling cellular-to-UAV path-loss for suburban environments," *IEEE Wireless Communications Letters*, vol. 7, no. 1, pp. 82–85, Feb. 2018.

[6] Q. Wu, Y. Zeng, and R. Zhang, "Joint trajectory and communication design for multi-UAV enabled wireless networks," *IEEE Transactions on Wireless Communications*, vol. 17, no. 3, pp. 2109–2121, Mar. 2018.

[7] M. Ding and D. López-Pérez, "Please lower small cell antenna heights in 5G," in *2016 IEEE Global Communications Conference (GLOBECOM)*, Dec. 2016, pp. 1–6.

[8] J. Li, H. Chen, Y. Chen, Z. Lin, B. Vucetic, and L. Hanzo, "Pricing and resource allocation via game theory for a small-cell video caching system," *IEEE Journal on Selected Areas in Communications*, vol. 34, no. 8, pp. 2115–2129, Aug 2016.

[9] J. Li, Y. Chen, Z. Lin, W. Chen, B. Vucetic, and L. Hanzo, "Distributed caching for data dissemination in the downlink of heterogeneous networks," *IEEE Transactions on Communications*, vol. 63, no. 10, pp. 3553–3568, Oct 2015.

[10] S. Lee and K. Huang, "Coverage and economy of cellular networks with many base stations," *IEEE Communications Letters*, vol. 16, no. 7, pp. 1038–1040, Jul. 2012.

[11] M. Ding, D. López-Pérez, G. Mao, and Z. Lin, "Study on the idle mode capability with LoS and NLoS transmissions," in *2016 IEEE Global Communications Conference (GLOBECOM)*, Dec. 2016, pp. 1–6.

[12] C. Ma, M. Ding, D. López-Pérez, Z. Lin, J. Li, and G. Mao, "Performance analysis of the idle mode capability in a dense heterogeneous cellular network," *IEEE Transactions on Communications*, vol. 66, no. 9, pp. 3959–3973, Sep. 2018.

[13] D. López-Pérez, M. Ding, H. Li, L. Galati-Giordano, G. Geraci, A. Garcia-Rodriguez, Z. Lin, and M. Hassan, "On the downlink performance of unmanned aerial vehicle communications in dense cellular networks," in *2018 IEEE Global Communications Conference (GLOBECOM)*, Dec. 2018.

[14] M. Ding, D. López-Pérez, G. Mao, and Z. Lin, "Performance impact of idle mode capability on dense small cell networks," *IEEE Transactions on Vehicular Technology*, vol. 66, no. 11, pp. 10 446–10 460, Nov. 2017.

[15] G. T. R. 36.777, "Technical specification group radio access network: Study on enhanced LTE support for aerial vehicles (Release 15)," Dec. 2017.

[16] M. Ding and D. López-Pérez, "Performance impact of base station antenna heights in dense cellular networks," *IEEE Transactions on Wireless Communications*, vol. 16, no. 12, pp. 8147–8161, Dec. 2017.